[American Journal of Science, Vol. 313, October, 2013, P. 790–806, DOI 10.2475/11.2013.01]

EROSIONAL RESPONSE TO NORTHWARD-PROPAGATING CRUSTAL THICKENING IN THE COASTAL RANGES OF THE U.S. PACIFIC NORTHWEST

GREG BALCO*,§,†, NOAH FINNEGAN**,§, ANDREW GENDASZEK***,§, JOHN O. H. STONE***,§, and NATHANIEL THOMPSON***,§

ABSTRACT. We measured basin-scale erosion rates, using cosmogenic ^{10}Be concentrations in quartz, from fluvial sediment in rivers draining the coastal mountain ranges of the U.S. Pacific Northwest between 40° and 47° N. Apparent erosion rates are 0.1 to 0.2 mm yr^{-1} throughout the Oregon Coast Ranges north of 43° N, and increase to the south to 0.6 to 1.1 mm yr^{-1} in the northern California coast ranges near 40° N. We propose that these observations display the erosional response to northward-migrating crustal thickening associated with subduction of the Mendocino Triple Junction. North-south variations in erosion rate, range elevation, and metrics of landscape relief and steepness are consistent with the hypotheses that i) their primary cause is northward-migrating crustal thickening; ii) erosion rates are strongly controlled by topographic relief and weakly, if at all, controlled by climate; and iii) the dependence of erosion on relief is nonlinear and obeys a threshold-relief relationship.

Key words: California, Oregon, U.S. Pacific Northwest, erosion rates, beryllium-10, cosmogenic-nuclide geochemistry, landscape evolution

INTRODUCTION

The Pacific coast of the northwestern United States traverses a series of coastal mountain ranges that are, in broad terms, the subaerial portion of the forearc of the Cascadia subduction zone. In northernmost California, Oregon, and Washington, they are the result of oblique convergence between the downgoing Juan de Fuca plate and overriding North America. Presumably, the topography of the coastal ranges in these regions is the result of transpressional rock uplift associated with this convergence. Farther south, in the higher topography of the coastal ranges of north-central California, the kinematics are significantly more complex due to subduction of the Mendocino triple junction (MTJ), which currently underlies Cape Mendocino (fig. 1). Furlong and Govers (1999) and Furlong and Schwartz (2004) synthesized observations of the tectonics of this region with a numerical model of crustal deformation, and proposed that the topography and tectonics of these ranges were best explained by a northward-migrating zone of transient crustal thickening and dynamic topography caused by viscous coupling between the North American and Gorda plates south of the MTJ. Subsequently, Lock and others (2006) showed that the uplift field predicted by this model (henceforth, the "Mendocino Crustal Conveyor" or "MCC" model following Lock and others) was consistent with geological evidence for rock uplift and deformation, and provided a good explanation for many features of the surface topography, present drainage pattern, and drainage evolution of the north-central California coast ranges.

The MCC model predicts that as the MTJ moves north, regions north of the MTJ will experience a transient increase in rock uplift rate from some background rate associated with steady plate convergence to a higher rate associated with crustal thickening above and in advance of the MTJ. In this paper we describe a set of

* Berkeley Geochronology Center, 2455 Ridge Road, Berkeley, California 94709 USA
** Earth and Planetary Sciences, University of California, Santa Cruz, California 95064 USA
*** Earth and Space Sciences, University of Washington, Seattle, Washington 98195 USA
§ Authors contributed equally. Listed in alphabetical order.
† Corresponding author: balcs@bgc.org

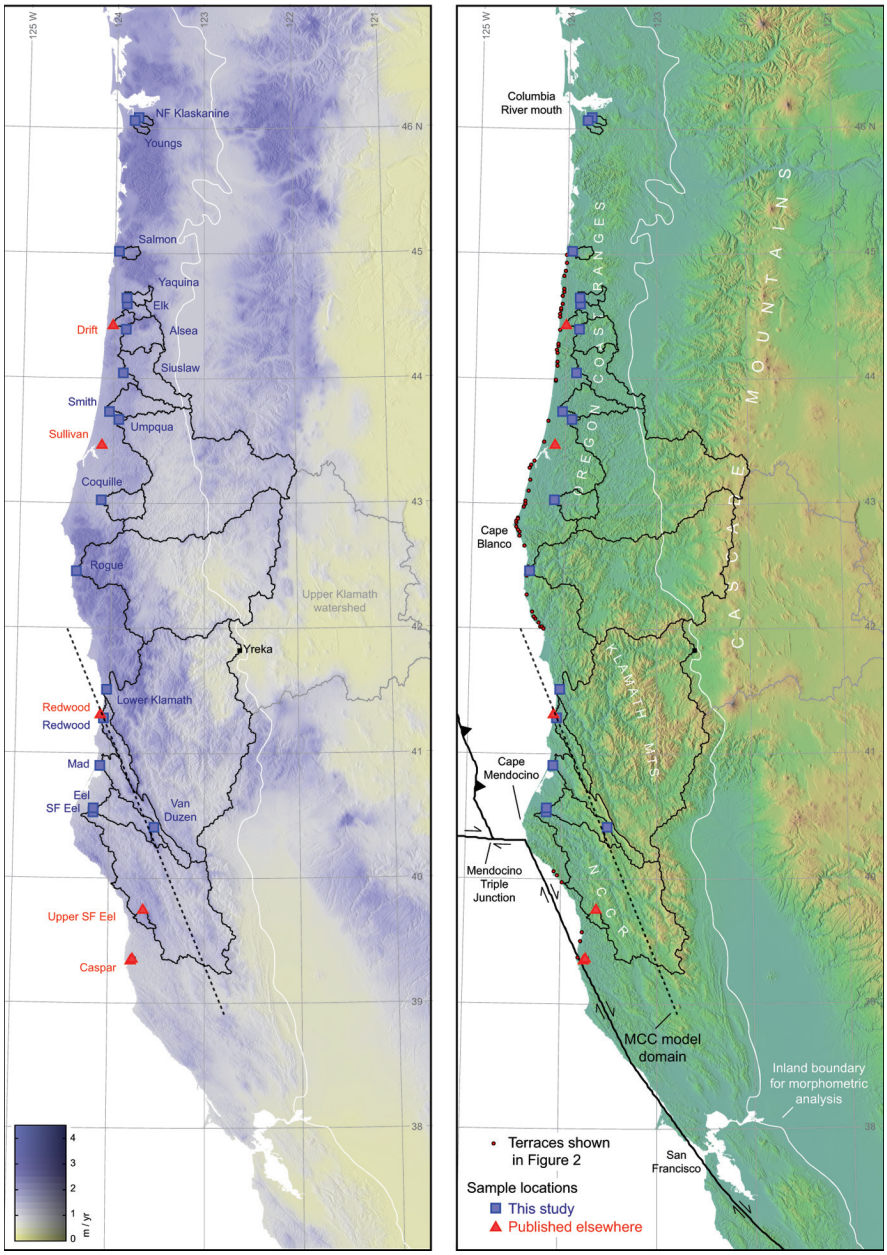

Fig. 1. Physiography and climate of the U.S. Pacific Northwest Coast Ranges. Map on right shows shaded-relief topography from the 90-M CGIAR-CSI SRTM digital elevation model (srtm.csi.cgiar.org); map on left shows 1971–2000 mean annual precipitation from the PRISM model (www.prism.oregonstate.edu). The white line on both maps shows the inland boundary of the coastal ranges that we used for the morphometric analyses shown in figure 2; where the physiographic boundary of the Coast Ranges is not obvious (in the Klamath highlands), this follows the eastern boundary of Cascades volcanic rocks. Symbols show sample locations for this study as well as comparable, previously published studies; black lines outline watersheds corresponding to our and others' samples. Note that watersheds for some samples overlap in the southern part of the study area: the Van Duzen and South Fork Eel catchments are part of the entire Eel catchment. The upper Klamath catchment, which is not included in calculating an erosion rate from the ^{10}Be concentration in the sample from the lower Klamath (see text), is outlined in gray. The dashed line shows the domain of the 2-dimensional numerical model (the "MCC model") of Furlong and Govers (1999). Red dots show location of uplifted terraces plotted in figure 3. Plate boundaries shown in right panel are from Bird (2003).

basin-scale erosion rate estimates derived from cosmogenic ^{10}Be measurements in sediment from coastal rivers between northernmost Oregon and north-central California. We propose that these data provide a synoptic view of the erosional response to the northward-migrating transient in rock uplift. Specifically, we argue that the observed distribution of erosion rates can be explained by i) a northward-migrating uplift field, similar to that predicted by the MCC model, superimposed on a background uplift rate associated with steady plate convergence; ii) consequent variations in the topography of the coastal ranges; and iii) a nonlinear relationship between topographic relief and erosion rates. In addition, this set of hypotheses implies that rock uplift exceeds erosion in much of the Coast Range in the vicinity of the MTJ. Our results suggest several ways to determine whether this is the case using field observations.

The Coastal Ranges of Northern California and Oregon

We are concerned with the coastal ranges between the Columbia River and Cape Mendocino, which include physiographic regions commonly described as the Oregon Coast Range (*ca.* 43°-46° N), the Klamath Mountains (*ca.* 41°-43° N), and the Northern California Coast Ranges (*ca.* 38°-41° N; see fig. 1). Pleistocene glaciation in the Coast Ranges has only significantly modified the landscape in a small area of high topography in the eastern Klamath Mountains near 41° N; otherwise glaciation has been minimal and confined to a few summits (Sharp, 1960). Hillslopes are typically soil-mantled and both shallow- and deep-seated landslides are common. Channel-forming processes include both rivers in low-gradient channels and debris flows in higher-gradient channels (for example, Stock and Dietrich, 2003). The Oregon Coast Range is composed mainly of siltstones and sandstones of the Eocene Tyee Formation (Dott and Bird, 1979), which emerged due to syn-subduction uplift in the Miocene (McNeill and others, 2000). This region has the wettest climate in the study area, with annual rainfall approaching 3 m/yr. The Klamath Mountains include older and more competent meta-sedimentary and plutonic rocks of Paleozoic and Mesozoic age (Irwin, 1960). The Northern California Coast Ranges are composed of a diverse set of rock types of the Franciscan Complex, which mainly includes poorly consolidated accretionary mèlange and some more competent sandstone units (Blake and others, 1985). Rivers draining the Northern California Coast Ranges deliver some of the highest sediment yields observed in the continental U.S. (Judson and Ritter, 1964). Summit elevations in the coastal ranges are near 1000 m in Oregon between 43° to 47° N, rise to 2000 to 2500 m in the Klamath Mountains and Northern California coast ranges between 39° and 42° N, and then decrease rapidly south of 42° N (figs. 1 and 2).

Cosmogenic-Nuclide Measurements of Basin-scale Erosion Rates

We measured basin-scale erosion rates in 16 coastal rivers (fig. 1; table 1) by analyzing cosmic-ray-produced ^{10}Be in quartz extracted from river sediment. Nearly all the cosmic ray flux stops in the first few meters below the Earth's surface, so nearly all production of ^{10}Be takes place in this zone. Given steady erosion of a surface, the residence time of rock or soil particles in the zone of ^{10}Be production as they are exhumed is inversely proportional to the erosion rate, so the ^{10}Be concentration in the resulting sediment is also inversely proportional to the erosion rate. Brown and others (1995), Bierman and Steig (1996), and Granger and others (1996) showed that this relationship is true at the drainage basin scale, so, subject to several assumptions, the ^{10}Be concentration in detrital quartz can be used to determine the average erosion rate in the catchment from which the quartz is derived.

We separated quartz from river sediment samples by wet-sieving to an appropriate grain-size range (mostly 0.25-0.5 mm; see table 1) and repeated etching in dilute HF. We then extracted Be from quartz using standard methods of HF dissolution and column chromatography (Stone and others, 2004). We used ^{9}Be carrier solutions

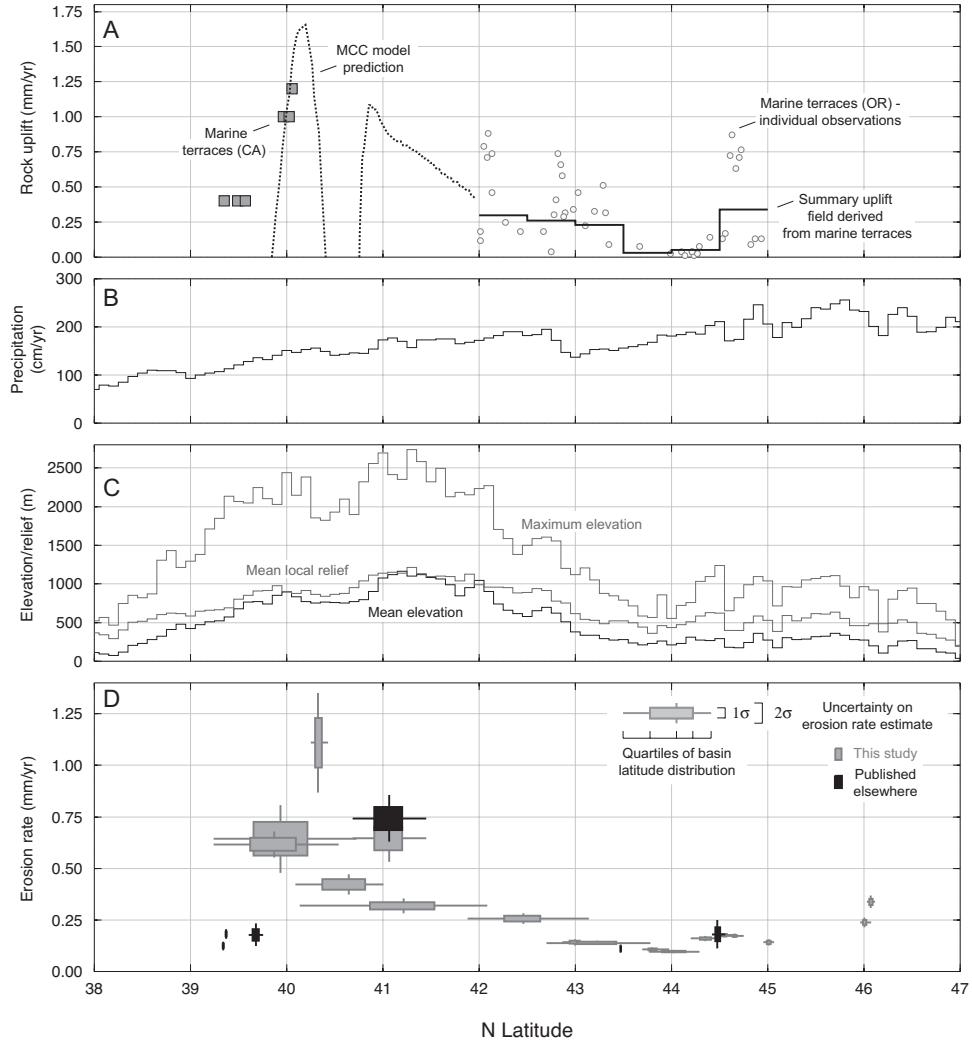

Fig. 2. Latitudinal variation in morphometry, climate, rock uplift rate, and apparent erosion rate for the Coast Ranges. (A) Selected rock uplift rate estimates based on marine terraces (McLaughlin and others, 1983; Merritts and Bull, 1989; Kelsey and others, 1994) with the uplift rate field predicted by the MCC model (Furlong and Govers, 1999; Lock and others, 2006). (B) Zonally averaged mean annual precipitation for the Coast Ranges, from the PRISM data shown in figure 1. (C) Zonally averaged maximum elevation, mean elevation, and 10-km-radius mean local relief for the Coast Ranges, all computed from the 90-m DEM shown in figure 1. (D) Apparent basin-scale erosion rates computed from ^{10}Be measurements. The latitudinal extent of boxes and lines denotes quartiles of the latitudinal distribution of basin area. Their vertical extent denotes 1- and 2-standard-error uncertainties on erosion rate estimates (external uncertainties of Balco and others, 2008; see table 1). Figure 1 shows the calculation domain for zonal averages in panels (B) and (C).

derived from deep-mined beryl with $^{10}Be/^{9}Be = 2–10 \times 10^{-16}$, and measured $^{10}Be/^{9}Be$ ratios by accelerator mass spectrometry at the Center for Accelerator Mass Spectrometry, Lawrence Livermore National Laboratory. Total process blanks were 4000 to 8000 atoms ^{10}Be, which represented 2 to 8 percent of the total number of atoms analyzed in any particular sample. Be isotope ratios were normalized at the time of measurement to the standards KNSTD3110 and LLNL3000 (table 1). To calculate

TABLE 1

Sample locations, ^{10}Be concentrations, apparent basin-scale erosion rates, and watershed properties required for erosion rate calculations or shown in figures

Sample name	Watershed name	Sample Location		Grain size (mm)	^{10}Be concentration (atoms g^{-1})	Be AMS standardization[1]	Watershed mean latitude (DD)	Watershed mean elevation (m)	Watershed effective elevation[2] (m)	Watershed apparent basin-scale erosion rate[5] (m Myr^{-1})	Watershed area (km^2)	Watershed mean local relief[3] (m)	Watershed steepness index k_{sn}[4]
		Latitude	Longitude										
New data from this study													
03-INQ-008-VDUS	Van Duzen River	40.417	-123.518	0.25-0.5	9582±1030	KNSTD	40.33	1172	1187	1109.8±142.5	150	879	43.2
03-INQ-015-EEL	South Fork Eel River	40.535	-124.156	0.25-0.5	13914±710	KNSTD	39.87 7	87	846	616.5±51.3	8150	915	77.3
03-INQ-017-EEL	Eel River	40.568	-124.155	0.25-0.5	13877±1741	LLNL3000	39.94	779	917	643.5±92.4	9265	905	75.0
03-INQ-019-MAD	Mad River	40.917	-124.090	0.25-0.5	20631±1208	KNSTD	40.60	811	865	422.4±37.4	1265	901	78.0
03-INQ-022-RWD	Redwood Creek[6]	41.289	-124.058	0.25-0.5	12171±1060	LLNL3000	41.06	574	608	645.9±70.2	714	870	65.1
03-INQ-024-KLM	Klamath River	41.518	-124.031	0.25-0.5	35018±1974	LLNL3000	41.19	1126	1190	318.7±28.5	16879	n/a	n/a
03-INQ-027-ROG	Rogue River	42.465	-124.369	0.25-0.5	36385±1870	KNSTD	42.45	898	958	256.7±21.8	13292	890	72.6
03-INQ-030-CQL	Coquille RIver	43.033	-124.114	0.25-0.5	51019±2601	LLNL3000	42.99	470	487	141.8±11.7	798	736	56.4
03-INQ-033-UMP	Umpqua River	43.678	-123.933	0.25-0.5	59409±2085	KNSTD	43.22	694	765	138.7±10.5	10893	756	57.7
03-INQ-035-SMI	Smith River	43.743	-124.037	0.25-0.5	56689±2533	KNSTD	43.81	282	287	107.2±8.4	910	460 3	0.4
03-INQ-036-SSL	Siuslaw River	44.051	-123.886	0.25-0.5	63395±2364	KNSTD	44.02	303	307	96.8±7.2	1538	474	21.9
03-INQ-037-ALS-O	Alsea River	44.399	-123.860	0.125-0.25	41346±1517	KNSTD	44.35	338	349	155.3±11.4	895	705	33.0
03-INQ-037-ALS-P	Alsea River	44.399	-123.860	0.25-0.5	40758±1673	KNSTD	44.35	338	349 1	57.6±12.0	895	705	33.0
03-INQ-037-ALS-Q	Alsea River	44.399	-123.860	0.5-0.85	38367±1856	KNSTD	44.35	338	349	167.7±13.4	895	705	33.0
04-NWR-002-ELK	Elk River	44.603	-123.852	0.25-0.5	34276±1027	KNSTD	44.55	245	250	176.8±12.3	220	581	22.6
04-NWR-003-YAQ	Yaquina River	44.651	-123.857	0.25-0.5	33871±1030	KNSTD	44.66	194	198	173.2±12.0	209	427	17.7
04-NWR-005-SAL	Salmon River	45.023	-123.945	0.25-0.5	47100±2480	KNSTD	45.01	380	402	141.2±11.8	155	765	51.5
04-NWR-015-YNG	Youngs River	46.070	-123.786	0.25-0.5	26591±1306	KNSTD	46.01	291	297	238.8±19.1	88	690	30.4
04-NWR-016-NFK	North Fork Klaskanine River	46.094	-123.739	0.25-0.5	18625±812	KNSTD	46.07	267	273	337.9±25.7	69	603	47.5
Data published elsewhere, recalculated with the same calculation methods used in this study													
DC22 (Bierman and others, 2001)	Drift Creek	44.428	-124.005	0.25-1	37000±13000	KNSTD	44.48	333	341	180.71±34.04	178	680	32.3
OR16 (Heimsath and others, 2001)	Sullivan Creek	43.470	-124.113	< 1	55540±4972	KNSTD	43.47	298	299	111.22±9.89	4	463	56.8
SFC (Ferrier and others, 2005)	South Fork Caspar Creek	39.346	-123.755	0.25-0.5	44900±3600	KNSTD	39.34	188	189	124.21±10.19	4	331	34.6
NFC (Ferrier and others, 2005)	North Fork Caspar Creek	39.360	-123.735	0.25-0.5	31600±2000	KNSTD	39.37	222	222	182.44±11.72	5	317	35.0
ORK (Ferrier and others, 2005)	Redwood Creek[6]	41.289	-124.058	0.25-0.5	10600±800	LLNL3000	41.06	574	608	742.35±56.48	714	870	69.0
012 (Fuller and others, 2009)	Upper South Fork Eel River	39.753	-123.629	0.25-0.5	38800±5820	07KNSTD	39.68	675	683	177.73±27.51	152	832	32.0

[1] Standardization codes are defined in the online exposure age/erosion rate calculator of Balco and others (2008) at http://hess.ess.washington.edu. Also see Nishiizumi and others (2007).

[2] This is the elevation at which the ^{10}Be production rate at the mean basin latitude corresponds to the area-averaged production rate in the entire watershed. Calculated using the "St" scaling scheme of Balco and others (2008).

[3] Calculated following Montgomery and Brandon (2002).

[4] Calculated following Wobus and others (2006). See caption to figure 3 for details.

[5] Calculated using the online calculator of Balco and others (2008), version 2.2. Assumes a material density of 2.5 g cm^{-3}.

[6] These samples were collected at the same location independently and at different times.

erosion rates, we used the 90-m SRTM digital elevation model and the production rate scaling scheme of Stone (2000) to compute an effective latitude and elevation for each basin; these are the latitude and elevation at which the ^{10}Be production rate is the same as the average of the ^{10}Be production rates computed for all pixels in the basin. We then used the erosion rate calculation scheme of Balco and others (2008) with the production rate calibration data set described therein. This calculation includes a renormalization of ^{10}Be measurements to the 07KNSTD standard series (see Nishiizumi and others, 2007). In addition, it takes into account ^{10}Be production by both spallation and muon reactions. As some previously published erosion rate estimates based on ^{10}Be measurements from our study area did not include both of these production pathways, we recalculated these (see table 1) using the same method. Thus, some of the erosion rate estimates reported in table 1 differ from previously published values.

Figure 1 and table 1 show sample locations, ^{10}Be concentrations, and erosion rate estimates inferred therefrom. Erosion rate estimates shown in table 1 and discussed henceforth are "apparent erosion rates," that is, they are computed on the basis that ^{10}Be concentrations in our study watersheds have reached equilibrium with a steady erosion rate. Several additional assumptions involved in this calculation are discussed at length in Bierman and Nichols (2004), von Blanckenburg (2006), and Balco and others (2008); we summarize the most relevant here.

The most important assumption for our data set is that all the sediment generated by surface erosion is evacuated from the catchment on a relatively short time scale. In other words, we assume that transfer of sediment in and out of long-term storage in the form of terraces, floodplains, or depositional basins is insignificant relative to the total sediment flux. This assumption is supported in our study by the fact that, with one significant exception, our study basins in the Coast Ranges consist nearly entirely of hillslopes and bedrock channels, and floodplains or terraces make up a negligible fraction of the basin area (also see discussion in Ferrier and others, 2005). In addition, we chose sample sites in confined bedrock channels upstream of tidal influence and extensive floodplains or estuaries. The exception is the Klamath River watershed (fig. 1), which is much larger than our other study watersheds, and the majority of which extends well past the eastern margin of the coastal ranges into intermontane sedimentary basins. The basins in the upstream Klamath drainage are sites of Quaternary and, presumably, ongoing, sediment accumulation, so the assumption of insignificant storage does not hold for the Klamath watershed. We sought to address this by assuming that sediment generated upstream of sedimentary basins is completely trapped, so only the portion of the Klamath watershed that is below the lowest sedimentary basin (specifically, below a dam at Yreka, CA; see fig. 1), contributes sediment to our sample site. If this assumption is true, then our erosion rate estimate should accurately represent the average erosion rate for the lower portion of the Klamath watershed that lies within the coastal ranges. Although the erosion rate calculated in this way is similar to apparent erosion rates in adjacent Coast Ranges watersheds (fig. 2), this assumption has a large effect on the result and we have not included the erosion rate estimate for the Klamath River in any further discussion or analysis. Two other relatively large watersheds, the Rogue and Umpqua watersheds, also extend past the Coast Ranges into the Cascades. Quaternary sedimentary basins in these watersheds, although present, are small relative to those in the upper Klamath watershed and make up a small fraction of these two watersheds. Thus, it is possible that sediment in these two watersheds is also disproportionately sourced in the Coast Ranges, rather than Cascades, portion of the watersheds. However, in contrast to the Klamath example, these watersheds lie predominantly within the Coast Ranges, and we found that whether or not we included the portions lying in the Cascades for purposes

of production rate calculations did not have a significant effect on the resulting erosion rate estimates. This issue could be resolved by collecting additional sediment samples representative of the headwaters of these basins.

BASIN-SCALE EROSION RATES IN THE COASTAL RANGES

Apparent basin-scale erosion rates inferred from ^{10}Be measurements are near 0.3 mm/yr in the northern Oregon Coast Ranges near 46° N and 0.1 to 0.15 mm/yr in the central Oregon Coast Ranges between 43° and 45° N (fig. 2; table 1). Southward of 43° N, apparent erosion rates increase by an order of magnitude, and the highest apparent erosion rate we observed is in the catchment of the Van Duzen River (a tributary of the Eel) near 40.5° N. Comparable, previously published measurements for the upper Eel (Fuller and others, 2009) and Caspar Creek (Ferrier and others, 2005) imply lower erosion rates, near 0.1 to 0.15 mm/yr, south of 40° N.

^{10}Be concentrations in multiple grain sizes from a single sample (from the Alsea River; see table 1) agree within measurement uncertainty.

Where our results overlap geographically with previously published results (those of Bierman and others, 2001 and Heimsath and others, 2001 for the central Oregon coast ranges and those of Ferrier and others, 2005 for Redwood Creek; see table 1 and fig. 2), they agree. We are not aware of any reason that they should not agree, but the agreement between independent studies that collected samples at different times and locations is noteworthy because there exist few, if any, attempts to independently replicate cosmogenic-nuclide erosion rate estimates.

As noted by numerous authors (Brown and others, 1995; Bierman and Steig, 1996; Schaller and others, 2002, 2004) an apparent erosion rate computed from a ^{10}Be concentration implies a time scale over which that erosion rate is integrated. This can be represented as an effective half-life for equilibration of the ^{10}Be concentration with the surface erosion rate, defined as $-ln(0.5)(\lambda + \varepsilon/\Lambda)^{-1}$ where λ is the ^{10}Be decay constant (yr^{-1}), ε is the erosion rate (g cm^{-2} yr^{-1}), and Λ is the effective attenuation length for spallogenic production (160 g cm^{-2}). For our results this time scale varies from 400 yr (Van Duzen River) to 4000 yr (central Oregon Coast Ranges). This is important because of evidence for changes in erosion and/or river incision rates in the Coast Ranges, presumably due to climate change, on glacial-interglacial time scales. Fuller and others (2009) showed that the erosion rate in a study basin in the upper Eel watershed 20,000 to 30,000 years ago was double the Holocene erosion rate; Wegmann and Pazzaglia (2002) showed that Holocene river incision rates in the adjacent Olympic Mountains of Washington were greater than incision rates averaged over entire glacial-interglacial cycles. The equilibration timescale for all the rivers in our study area appears to be short enough that our erosion rate estimates should correctly represent Holocene erosion rates. If this were not the case and, for example, our entire study area responded to climate change as shown for the Eel watershed by Fuller and others, then slower equilibration in study basins with lower erosion rates would result in an apparent north-south gradient in erosion rates that would underestimate the true gradient. In addition, the range of erosion rates we observe (a factor of 10) is larger than the temporal variations in erosion rate observed by Fuller and others (a factor of 2) or those in incision rate observed by Wegmann and Pazzaglia (a factor of 2-3). Thus, the existence of glacial-interglacial variation in erosion rates does not by itself affect the conclusion that there is a significant north-south gradient in erosion rates in the Coast Ranges.

Erosion Rates Compared to Climate

Mean annual precipitation in the Coast Ranges decreases from 2.5 m yr^{-1} in the northern Oregon Coast Range to 1 m yr^{-1} in the Northern California Coast Ranges (figs. 1 and 2). The average number of days of rainfall decreases correspondingly, from

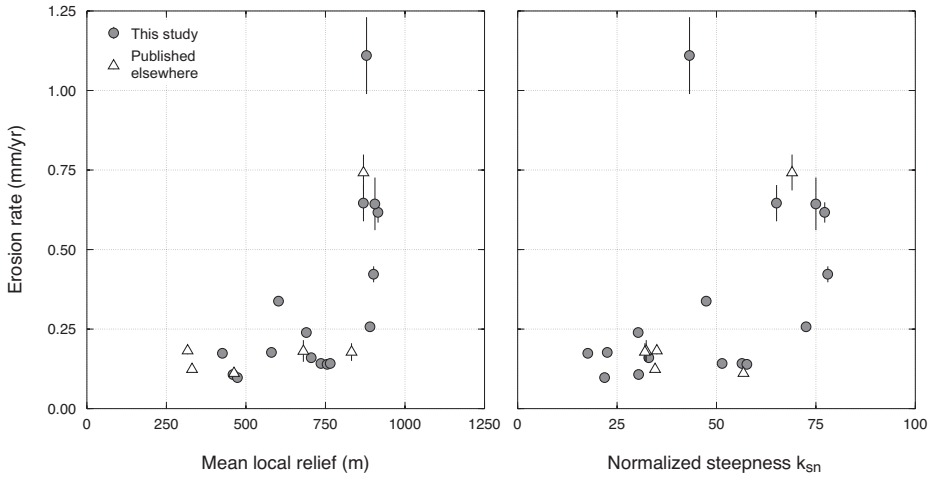

Fig. 3. Relationship between apparent erosion rate computed from ^{10}Be measurements and steepness/relief metrics for study basins. Mean local relief is computed from the 90-m SRTM digital elevation model for a 10-km radius (for example, Montgomery and Brandon, 2002). Normalized channel steepness is calculated from a 10-m DEM according to Wobus and others, 2006, using a reference concavity of 0.45, a channel initiation threshold of 0.7 km^2, and calculation of river slope over a 10 m vertical interval. Error bars show internal uncertainties in erosion rate estimates (table 1); where not visible they are smaller than the symbol size.

220 days in the northern Oregon Coast Ranges to 120 days in the Eel River watershed, suppressing latitudinal variation in rainfall intensity (as, for example, defined by Wilson, 1997, and proposed as an important determinant of debris-flow activity). Erosion rates, on the other hand, increase from north to south, resulting in a weak negative correlation between precipitation or rainfall intensity and erosion rate. As there is no obvious physical mechanism suggesting such a negative correlation, we conclude that climate, at least as quantified by these parameters, is not the primary control on erosion rates in this region.

Erosion Rates Compared to Topography

Erosion rate covaries with topography and relief in the Coast Ranges. The lowest erosion rates we observed correspond to the relatively low-elevation topography of the central Oregon coast, whereas the highest erosion rates are associated with the high topography and relief of the Northern California Coast Ranges. This general observation is consistent with the idea that relief exerts a strong control on erosion rates (Ahnert, 1970). Figure 3 shows that the relationship between erosion rate and various metrics of relief or river steepness, for example the normalized channel steepness k_{sn} (Wobus and others, 2006) or the mean local relief (Montgomery and Brandon, 2002), is nonlinear. This nonlinear relationship resembles a so-called "threshold" model for the relationship between erosion and topographic relief, in which a linear relation between measures of relief and erosion at low relief is superseded by a decorrelation at high relief.

The "threshold" concept originated from observations of linear hillslope profiles in some landscapes (Penck, 1953), which suggest maintenance at a critical slope angle by landslides or other sediment transport processes whose rate is a nonlinear function of slope. Roering and others (2001) formalized a physical description of this concept for soil-mantled landscapes that are prone to shallow landsliding, such as are characteristic of our study area. In this model, erosion rates become independent of slope angle

and therefore of local relief as a critical slope angle is approached. Slopes near this critical angle respond to an increase in the rock uplift rate by an increase in the frequency of landsliding rather than a change in slope or, consequently, in relief. Thus, a soil-mantled landscape is expected to display a narrow range of local relief at high erosion rates and a wide range of local relief at low erosion rates. A number of studies that related erosion-rate measurements to morphometric parameters at a variety of scales (for example, Burbank and others, 1996; Montgomery, 2001; Montgomery and Brandon, 2002; Binnie and others, 2007; Ouimet and others, 2009; DiBiase and others, 2010) have observed this relationship. In fact, the observation, that erosion rates in mountain landscapes obey a threshold-type relationship to parameters describing river steepness or relief, is a fundamental discovery that has emerged from the development of the techniques of digital topographic analysis and cosmogenic-nuclide erosion rate estimates. This result does not depend strongly on the particular method of quantifying steepness or relief; in fact, DiBiase and others (2010) showed that commonly used such parameters are linearly related, so all show an equivalently nonlinear relationship to erosion rates.

To summarize, our data set for the Coast Ranges displays a nonlinear relationship between erosion rate and measures of topographic relief or river steepness that is consistent with a threshold-relief model. This is consistent with related observations from the region: in the Oregon Coast Range, Montgomery (2001) showed that mean slope angle (and therefore local relief) is correlated with rock uplift rate. Our measurements support this model in that they show that erosion rates generally increase with local relief in relatively low-relief and low-erosion-rate watersheds north of 43° N. In contrast, the correlation between relief and erosion rates breaks down in the Northern California Coast Ranges between 40° to 43° N, implying that this landscape has reached a critical relief such that changes in uplift rates can be balanced by changes in erosion rates without measurable adjustment of relief or steepness.

Erosion Rates Compared With Rock Uplift Rates

Rock uplift rates averaged over *ca.* 10,000-year timescales can be inferred from the elevation of marine terraces that have been mapped along much of the northwest Coastal Ranges. Published observations include those of Kelsey and others (1994) and references therein for Oregon, and Merritts and Bull (1989) and McLaughlin and others (1983) for California (figs. 1 and 2). Extraordinarily high rock uplift rates are recorded by terraces along the coastal King Range near 40° N (*ca.* 4 mm yr^{-1}), but the King Range is thought to be tectonically decoupled from inland regions (Blake and others, 1985), in which case rock uplift rates inferred from the King Range terraces would be unrelated to rock uplift rates in our study basins. Thus, we have not considered the King Range terraces further. In the Oregon Coast Range, rock uplift rates inferred from marine terraces are locally as high as 0.8 mm yr^{-1} at a few sites near major coastline-normal faults, but overall suggest regional rock uplift rates of ~0.1 mm yr^{-1} in the central Oregon Coast Range and ~0.2 to 0.3 mm yr^{-1} in the southern Oregon Coast Range (fig. 2). At the southern end of our study area south of Cape Mendocino, rock uplift rates inferred from marine terraces are 0.3 to 1.2 mm yr^{-1} (fig. 2).

The MCC model of Furlong and Govers (1999) provides an estimate of rock uplift rates for our study area between 40° to 42° N. This uplift field is the sum of long-wavelength isostatic uplift due to crustal thickening and shorter-wavelength variations due to the northward propagation of dynamic topography. Lock and others (2006) showed that this model uplift field is consistent with available geomorphic and stratigraphic data between 40° and 42° N, and it is consistent with rock uplift rates inferred from marine terraces near 42° N. Despite i) sensitivity of the predicted uplift rates to viscoelastic parameters in the model, and ii) some disagreement between model and geologic observations, for example the inconsistency between model

subsidence near 39° N and evidence of long-term uplift from marine terraces at this latitude, the MCC model provides the only physically based prediction of rock uplift rates in the Northern California Coast Range on the time scale addressed by our erosion rate estimates, that is, a time scale long enough to span multiple earthquake cycles.

In the central Oregon Coast Range, erosion rates and rock uplift rates inferred from marine terraces are both 0.1 to 0.25 mm yr^{-1} and display a similar latitudinal pattern, with a minimum in both erosion and uplift rates near 0.1 mm yr^{-1} at 44° N. Heimsath and others (2001) also noted the approximate correspondence between erosion and uplift rates in this region, as well as the consistency of erosion rates measured at different landscape scales, and suggested that this region represents an "approximate large-scale equilibrium," in which erosion and uplift are steady and balanced (see also Reneau and Dietrich, 1991, and Personius, 1995). Our results are consistent with this idea. In the Northern California Coast Ranges, the MCC model predicts large north-south variations in rock uplift rates, with an increase from 0.3 mm/yr near 42° N to *ca.* 1.5 mm yr^{-1} near 40° N, a zone of subsidence associated with dynamic topography near 40.5° N, and subsidence south of ~40° N. Our erosion rate estimates for this region have similar magnitude as the predicted uplift rates, ranging between 0.4 and 1.1 mm yr^{-1} The highest erosion rates we observed, in the headwaters of the Van Duzen River, occur at the latitude of highest predicted uplift rates.

Erosion Rates in the Context of Northward-propagating Crustal Thickening

Furlong and Govers (1999) and Lock and others (2006) argued that the high topography of the coastal Klamath Mountains and the Northern California coast ranges was the result of northward-propagating crustal thickening associated with the Mendocino triple junction. Because of the similarity among latitudinal patterns in predicted and observed uplift rates, elevation and relief, and apparent erosion rates (fig. 2), we hypothesize that the large variation in erosion rates that we observe also reflects the response of the landscape to transient crustal thickening. This hypothesis also implies that erosion rates and rock uplift rates are not in balance in much of the landscape, otherwise there would be no mechanism for increasing mean elevation in the vicinity of the MTJ. As the locus of crustal thickening moves north, rock uplift must be faster than erosion for the mean elevation of the Coast Ranges to increase in response.

Based on the results described above, we ask two questions. First, is observed variability in elevation, relief, and erosion rate consistent with the variation in rock uplift rates predicted by the MCC model and current understanding of the topographic controls on erosion rates? Second, what degree of disequilibrium between uplift and erosion is required to explain the observations, and is it possible to directly discern from our observations whether or not the Coast Ranges are a transient landscape? We attempt to shed some light on these questions by comparing observations to a simple, one-dimensional, model of landscape response to a transient pulse of rock uplift. By parameterizing the model with constants appropriate to the dimensions, uplift rates, and erosion rates of the Coast Ranges, we aim to show that even a highly simplified representation of this process duplicates the main features of our data set, and we propose that it provides a framework for understanding north-south variation in erosion rates and landscape metrics in the region.

The simplest possible model that illustrates the essential concepts of landscape response, as quantified by range elevation and erosion rate, to a transient change in uplift rate is the 1-d model:

$$\frac{\partial \bar{Z}}{\partial t} = U(t) - \varepsilon \tag{1}$$

where $\bar{Z}$ is mean range elevation (m), $U(t)$ is a prescribed uplift rate (m yr^{-1}) as a function of time t, and ε is the erosion rate (m yr^{-1}). To evaluate equation (1), we need a functional relationship between the mean elevation and the erosion rate. As we have already argued that the erosion rates we observe are governed by a threshold-relief-type model, we will use the relief parameterization and functional form of Montgomery and Brandon (2002):

$$\varepsilon = \varepsilon_0 + \frac{KR_z}{1 - (R_z/R_c)^2} \tag{2}$$

where ε_0 is a background erosion rate (m yr^{-1}), K is an empirical rate constant, R_z is mean local relief (m) (specifically, calculated on a 90-m DEM over a 10-km-diameter analysis window), and R_c is a critical relief (m). We estimate parameters appropriate for our study area from our data (fig. 4D). In addition, we must relate the mean local relief R_z to the mean elevation $\bar{Z}$. The form of equation (2) is common to many proposed nonlinear erosion laws (for example, Roering and others, 2007 and references therein). However, for our purposes, parameterizing the erosion rate in terms of mean local relief as defined by Montgomery and Brandon is advantageous because mean local relief in a relatively large window and mean elevation are related parameters—relief is limited by range elevation—and, in an approximately self-similar fluvially dissected landscape such as the Coast Ranges, they are expected to covary. This is in fact the case (fig. 4E), and we approximate this relationship for the Coast Ranges by:

$$R_z = a\bar{Z}^b \tag{3}$$

with appropriate parameter values (fig. 4E). Combining equations (1), (2), and (3) yields:

$$\frac{\partial \bar{Z}}{\partial t} = U(t) - \left[\varepsilon_0 + \frac{aK\bar{Z}^b}{1 - (a\bar{Z}^b/R_c)^2}\right] \tag{4}$$

Figure 4 (A-C) shows the changes in elevation, mean local relief, and erosion rate predicted by equation (4) when forced by a pulse of rock uplift with dimensions appropriate to the MCC model. The uplift rate function is intended to be a simple representation of the idea that a region of crustal thickening is moving northward with the MTJ. To generate this, we assume the following. First, we impose a constant background uplift rate of 0.1 mm yr^{-1}, which represents steady rock uplift associated with plate convergence prior to the onset of MTJ-associated crustal thickening. We then assume that the thickened region is Gaussian in shape, and relate model time to along-range distance using the northward velocity of the MTJ relative to stable North America. This implies a latitudinal distribution of uplift rates that is the sum of a constant background uplift rate and the first derivative of a Gaussian, and we chose the parameters of the function so that the lateral extent of the zone of transient uplift and the maximum uplift rate resembled those predicted by the MCC model (fig. 4). As our goal is to describe the basic topographic and erosion-rate implications of the idea that there is a northward-propagating transient in uplift rate—not to test or validate specific aspects of the MCC model—we did not attempt to exactly replicate the MCC model uplift field or incorporate its predicted short-wavelength dynamic topography.

Clearly equation (4) is a highly simplified description of topographic response to transient uplift. However, figure 4 shows that when the parameters of this model are chosen appropriately for the Coast Ranges, it duplicates the important features of our data set. First, a steady-state solution to equation (4) applies at the latitude of the Oregon Coast Range between 44° and 45° N, where MTJ-related rock uplift has not yet occurred. This implies an equilibrium landscape with mean elevation near 200 m and

erosion and uplift rates at the prescribed background uplift rate of 0.1 mm yr^{-1}. To the south, where equation (4) is forced by the prescribed transient uplift rate distribution, the model predicts a transition from this equilibrium region with mean elevation near 200 m, to a region with mean elevation near 800 m in the Northern California coast range near 40.5° N, which agrees with observations. Second, the model predicts that despite large variations in uplift and erosion rates between 39.5° and 41.5° N, the elevation of the Northern California coast ranges is fixed near a limiting height throughout this region by the nonlinearity of the relief-erosion rate relationship in equation (2). This agrees with the observation that apparent erosion rates in this region span almost an order of magnitude, but mean range elevation varies only slightly.

We conclude from this comparison that available observations of range morphometry, uplift rate, and erosion rate in the Coast Ranges are consistent with the three basic ideas that i) latitudinal variation in these quantities is primarily the result of northward-migrating crustal thickening associated with the MTJ; ii) topographic relief/steepness is the primary control on erosion rates in this region; and iii) the dependence of erosion on relief/steepness is nonlinear. If we start only with these three simple assumptions, we can successfully predict the most important features of our data set.

The model results in figure 4 also suggest several additional hypotheses about the landscape of the Coast Ranges, and shed some light on the question of whether it is possible to use geological and geochemical observations of rock uplift rates and erosion rates to distinguish steady-state and transient landscapes. Our argument that latitudinal variation in topography and erosion rates in the Coast Ranges is the result of northward-migrating crustal thickening implies that part of the range is actively growing. Figure 4 suggests that the approximate condition of equilibrium between uplift and erosion rates, that we and others have proposed for the Oregon coast ranges, is most likely the case only north of *ca.* 43° N. South of this latitude, uplift rates must significantly exceed erosion rates. If, in fact, the increase in mean range elevation from ~200 m near 43.5° N to ~ 1000 m near 41.5° N is a northward-propagating transient, then the elevation difference (~800 m), the N-S distance over which this increase takes place (~200 km) and the corresponding relative plate velocity (~50 km/Myr) imply that the uplift rate exeeded the erosion rate by an average of ~0.2 mm yr^{-1} over 4 Myr. The difference in rates must vary over time, and the parameters we used to evaluate equation (4) imply a maximum difference between uplift and erosion rates of *ca.* 0.25 mm yr^{-1}. Both of these estimates are several times greater than typical uncertainties in watershed-scale erosion rate estimates (table 1), and should also be much greater than the uncertainty in long-term uplift rate inferred from marine terraces associated with well-dated relative sea level changes. Thus, we propose that it would potentially be possible to use local measurements of erosion and uplift rates to quantitatively distinguish equilibrium from transient landscapes in a more geographically focused study. If this were successful, in turn, it would allow one to unambiguously identify topographic metrics that might be used to identify such transient landscapes in the absence of uplift and erosion rate measurements.

Oversimplifications, Weaknesses, and Potential Improvements

In the previous section we argued that available observations from the Coast Ranges were consistent with the hypothesis that the Coast Range landscape is the result of northward-migrating crustal thickening and a nonlinear relief-erosion relationship. However, our argument includes several important oversimplifications, and in addition we have not sought to test our hypothesis with additional supporting evidence that could easily be gathered. We discuss these deficiencies here to highlight the fact that correcting them would provide valuable and broadly interesting information.

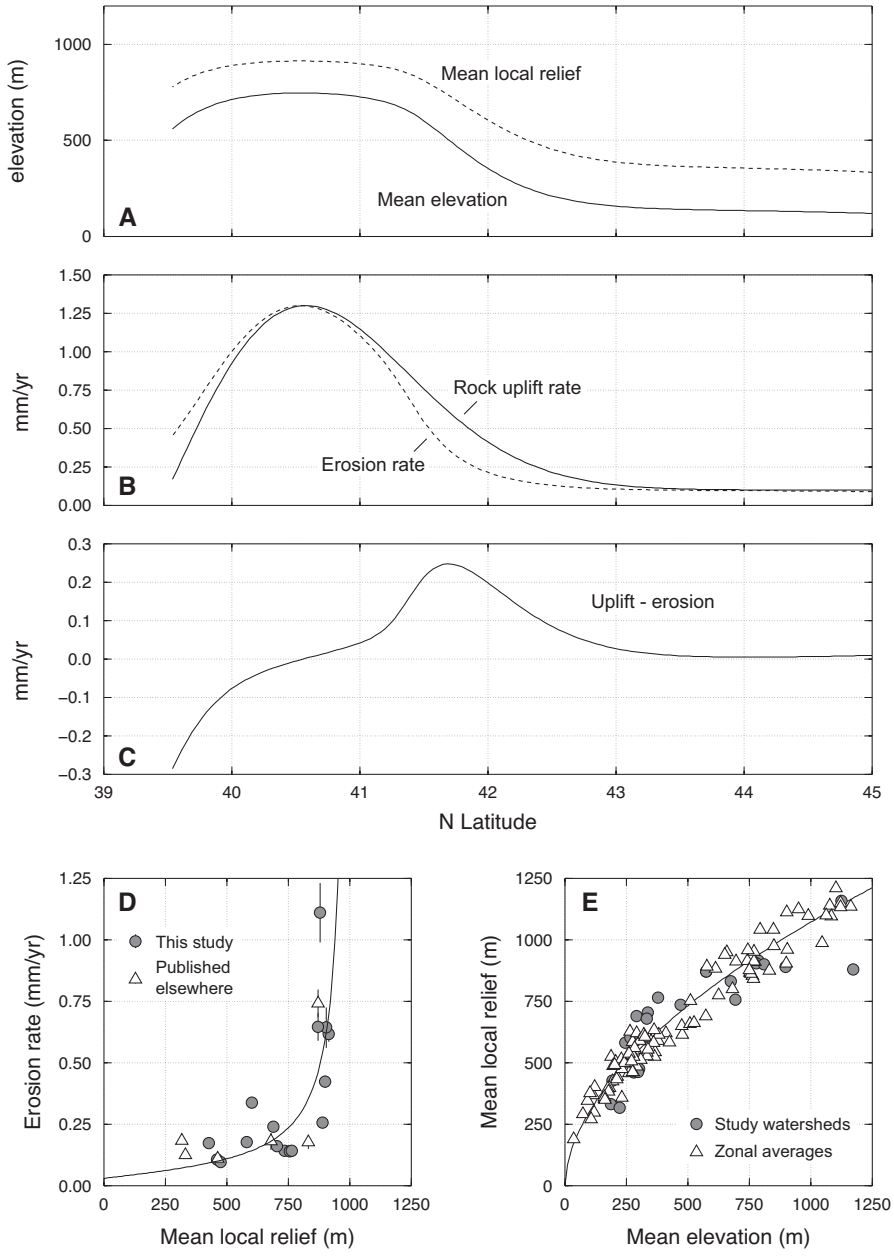

Fig. 4. Upper three panels, latitudinal distribution of mean elevation, mean local relief, and erosion rate for the Coast Ranges predicted by equation (4). Panel (A) shows predicted mean elevation and corresponding mean local relief. Both quantities are predicted to saturate at values near the critical relief in equation (2) and corresponding mean elevation, at latitudes corresponding to the Northern California coast ranges. Panel (B) shows the prescribed distribution of rock uplift rates and the consequent predicted distribution of erosion rates. As described in the text, the uplift rate function is the first derivative of a Gaussian with dimensions appropriate to the MCC model, added to a background uplift rate of 0.1 mm yr^{-1} that represents uplift due to plate convergence. Equation (4) then predicts the erosion rates shown by the dashed line. Note that predicted erosion rates continue to increase through the region where range elevation is limited by the threshold-relief dependence of the erosion rate. Panel (C) shows the difference between uplift and erosion rates predicted by equation 4. Lower two panels, data used to parameterize equation (4) appropriately for the Coast Ranges. The line in (D) shows the mean local relief–erosion rate

Our primary oversimplification is that, in preparing figure 2 and structuring our discussion around this figure, we have telescoped all variability in morphometry, uplift rate, and erosion rate into a single coast-parallel (north-south) dimension. In reality, the northward migration of the MTJ as well as tectonic processes not included in the MCC model, for example subduction of the Pacific plate and the overall accommodation of transpressional deformation throughout the Coast Ranges and Cascades, affect a variety of upper crustal structures that would be expected to impose significant variability in a coast-perpendicular (east-west) direction. For example, the Klamath Mountains topographic high is disproportionately wider than rest of the coastal ranges and, in fact, merges with the Cascades; it appears unlikely that this is predicted by the MCC model. Furthermore, presenting erosion rates for small coastal basins on the same axes in figure 2 as large basins that cross the entire range and extend eastward to the Cascade foothills may improperly conflate N-S and E-W variability in our data set. Addressing this simplification would require a more detailed representation of Coast Range tectonics, a three-dimensional model of deformation due to oblique convergence in the MTJ region, and additional erosion rate estimates from smaller basins designed to capture east-west variability in erosion rates.

A secondary oversimplification is that we have ignored the fact that the relief-erosion relationship is likely to differ with lithological variations among the Oregon Coast Ranges, the Klamath Mountains, and the Northern California coast ranges. Again, this issue could be addressed by a more spatially detailed erosion rate study.

Third, we have argued that north-south variations in climate are not the primary cause of erosion rate variability, and not considered them further. However, these variations do presumably exert a second-order effect on the magnitude and distribution of geomorphic processes active within the Coast Ranges; this likelihood is further supported by the observation that glacial-interglacial climate change appears to affect erosion rates (Wegmann and Pazzaglia, 2002; Fuller and others, 2009).

The main deficiency in supporting evidence for our hypothesis is as follows. We have proposed that a transition from non-threshold to threshold landscapes occurs at the point where morphometric parameters saturate with respect to uplift and erosion rate. However, we have not shown from a process perspective that this is true. We expect that this transition will be accompanied by such phenomena as, for example, an increase in landslide extent and frequency or an increased incidence of linear slopes (for example, Roering and others, 2007; Hilley and Arrowsmith, 2008). In addition, transitional regions of the central Coast Ranges where we hypothesize that uplift rates exceed erosion rates may well show some topographic signature of this condition, including disturbed river long profiles (for example, Crosby and Staiger, 2007) or the formation of inner gorges (Kelsey, 1988). We have not looked in detail for any of these features.

CONCLUSIONS

Erosion rate estimates and morphometric observations for the U.S. Pacific Northwest Coast Ranges between 40° and 47° N display the erosional response to northward-migrating crustal thickening associated with the MTJ. North-south variations in erosion rate, range elevation, and metrics of landscape relief and steepness are consistent with the hypotheses that i) their primary cause is northward-migrating crustal thickening; ii) erosion rates are strongly controlled by topographic relief and weakly, if at all,

relationship given by equation (2) with parameters $\varepsilon_0 = 0.03$ m yr^{-1}, $K = 0.00012$, and $R_c = 1000$ m. The data points are the same as in figure 3. The line in (E) shows the relationship between mean elevation and mean local relief represented by equation (3) with $a = 24$ and $b = 0.55$. Triangles show data derived from the 90-m DEM for the 0.1° zonal bins shown on figure 2, and circles are corresponding data for study watersheds.

controlled by climate; and iii) the dependence of erosion on relief is nonlinear and obeys a threshold-relief relationship.

ACKNOWLEDGMENTS

We thank Devin McPhillips, Mark Brandon, and an anonymous reviewer for helpful and comprehensive reviews.

References

Ahnert, F., 1970, Functional relationships between denudation, relief, and uplift in large midlatitude drainage basins: American Journal of Science, v. 268, n. 3, p. 243–263, http://dx.doi.org/10.2475/ajs.268.3.243

Balco, G., Stone, J. O., Lifton, N. A., and Dunai, T. J., 2008, A complete and easily accessible means of calculating surface exposure ages or erosion rates from ^{10}Be and ^{26}Al measurements: Quaternary Geochronology, v. 3, n. 3, p. 174–195, http://dx.doi.org/10.1016/j.quageo.2007.12.001

Bierman, P., and Steig, E. J., 1996, Estimating rates of denudation using cosmogenic isotope abundances in sediment: Earth Surface Processes and Landforms, v. 21, n. 2, p. 125–139, http://dx.doi.org/10.1002/(SICI)1096-9837(199602)21:2⟨125::AID-ESP511⟩3.0.CO;2-8

Bierman, P. R., and Nichols, K. K., 2004, Rock to sediment, Slope to sea with ^{10}Be, Rates of landscape change: Annual Reviews of Earth and Planetary Sciences, v. 32, p. 215–255, http://dx.doi.org/10.1146/annurev.earth.32.101802.120539

Bierman, P. R., Clapp, E. M., Nichols, K., Gillespie, A., and Caffee, M. W., 2001, Using cosmogenic nuclide measurements in sediments to understand background rates of erosion and sediment transport *in* Harmon, R. S., and Doe, W. M., editors, Landscape Erosion and Evolution Modeling: New York, Kluwer, p. 89–116.

Binnie, S. A., Phillips, W. M., Summerfield, M. A., and Fifield, L. K., 2007, Tectonic uplift, threshold hillslopes, and denudation rates in a developing mountain range: Geology, v. 35, n. 8, p. 743–746, http://dx.doi.org/10.1130/G23641A.1

Bird, P., 2003, An updated digital model of plate boundaries: Geochemistry, Geophysics, Geosystems, v. 4, n. 3, p. 1027, http://dx.doi.org/10.1029/2001GC000252

Blake, M. C., Jayko, A. S., and McLaughlin, R. J., 1985, Tectonostratigraphic terranes of the northern Coast Ranges, California *in* Howell, D. G., editor, Tectonostratigraphic terranes of the circum-Pacific region: Houston, Texas, Circum-Pacific Council for Energy and Mineral Resources, p. 159–186.

Brown, E. T., Stallard, R. F., Larsen, M. C., Raisbeck, G. M., and Yiou, F., 1995, Denudation rates determined from the accumulation of *in-situ*-produced ^{10}Be in the Luquillo Experimental Forest, Puerto Rico: Earth and Planetary Science Letters, v. 129, n. 1–4, p. 193–202, http://dx.doi.org/10.1016/0012-821X(94)00249-X

Burbank, D. W., Leland, J., Fielding, E., Anderson, R. S., Brozovic, N., Reid, M. R., and Duncan, C., 1996, Bedrock incision, rock uplift and threshold hillslopes in the northwestern Himalayas: Nature, v. 379, p. 505–510, http://dx.doi.org/10.1038/379505a0

Crosby, B. T., and Staiger, J. W., 2007, Evaluating the crustal conveyor: an analysis of terraces and channel profiles along the South Fork Eel River, northern California: Geological Society of America Abstracts with Programs (2007 Annual Meeting), v. 39, p. 262.

DiBiase, R. A., Whipple, K. X., Heimsath, A. M., and Ouimet, W. B., 2010, Landscape form and millennial erosion rates in the San Gabriel Mountains, CA: Earth and Planetary Science Letters, v. 289, n. 1–2, p. 134–144, http://dx.doi.org/10.1016/j.epsl.2009.10.036

Dott, R. H., Jr., and Bird, K. J., 1979, Sand transport through channels across an Eocene shelf and slope in southwestern Oregon, U.S.A., *in* Doyle, L. J., and Pilkey, O. H., editors, Geology of continental slopes: Society for Economic Paleontologists and Mineralogists Special Publication n. 27, p. 327–342, http://dx.doi.org/10.2110/pec.79.27.0327

Ferrier, K. L., Kirchner, J. W., and Finkel, R. C., 2005, Erosion rates over millennial and decadal timescales at Caspar Creek and Redwood Creek, Northern California Coast Ranges: Earth Surface Processes and Landforms, v. 30, n. 8, p. 1025–1038, http://dx.doi.org/10.1002/esp.1260

Fuller, T. K., Perg, L. A., Willenbring, J. K., and Lepper, K., 2009, Field evidence for climate-driven changes in sediment supply leading to strath terrace formation: Geology, v. 37, n. 5, p. 467–470, http://dx.doi.org/10.1130/G25487A.1

Furlong, K. P., and Govers, R., 1999, Ephemeral crustal thickening at a triple junction: The Mendocino crustal conveyor: Geology, v. 27, n. 2, p. 127–130, http://dx.doi.org/10.1130/0091-7613(1999)027⟨0127:ECTAAT⟩2.3.CO;2

Furlong, K. P., and Schwartz, S. Y., 2004, Influence of the Mendocino Triple Junction on the tectonics of coastal California: Annual Reviews of Earth and Planetary Sciences, v. 32, p. 403–433, http://dx.doi.org/10.1146/annurev.earth.32.101802.120252

Granger, D. E., Kirchner, J. W., and Finkel, R., 1996, Spatially averaged long-term erosion rates measured from *in situ*-produced cosmogenic nuclides in alluvial sediment: Journal of Geology, v. 104, n. 3, p. 249–257, http://dx.doi.org/10.1086/629823

Heimsath, A. M., Dietrich, W. E., Nishiizumi, K., and Finkel, R. C., 2001, Stochastic processes of soil production and transport: Erosion rates, topographic variation and cosmogenic nuclides in the Oregon Coast Range: Earth Surface Processes and Landforms, v. 26, n. 5, p. 531–552, http://dx.doi.org/10.1002/esp.209

Hilley, G. E., and Arrowsmith, J. R., 2008, Geomorphic response to uplift along the Dragon's Back pressure ridge, Carrizo Plain, California: Geology, v. 36, n. 5, p. 367–370, http://dx.doi.org/10.1130/G24517A.1

Irwin, W. P., 1960, Geologic reconnaissance of the northern Coast Ranges and Klamath Mountains, California: California Division of Mines Bulletin, v. 179, 80 p.

Judson, S., and Ritter, D. F., 1964, Rates of regional denudation in the United States: Journal of Geophysical Research, v. 69, n. 16, p. 3395–3401, http://dx.doi.org/10.1029/JZ069i016p03395

Kelsey, H. M., 1988, Formation of inner gorges: Catena, v. 15, n. 5, p. 433–458, http://dx.doi.org/10.1016/0341-8162(88)90063-X

Kelsey, H. M., Engebretson, D. C., Mitchell, C. E., and Ticknor, R. L., 1994, Topographic form of the Coast Ranges of the Cascadia Margin in relation to coastal uplift rates and plate subduction: Journal of Geophysical Research—Solid Earth, v. 99, n. B6, p. 12245–12255, http://dx.doi.org/10.1029/93JB03236

Lock, J., Kelsey, H., Furlong, K., and Woolace, A., 2006, Late Neogene and Quaternary landscape evolution of the Northern California Coast Ranges: Evidence for Mendocino triple junction tectonics: Geological Society of America Bulletin, v. 118, n. 9–10, p. 1232–1246, http://dx.doi.org/10.1130/B25885.1

McLaughlin, R. J., Lajoie, K. R., Sorg, D. H., Morrison, S. D., and Wolfe, J. A., 1983, Tectonic uplift of a middle Wisconsin marine platform near the Mendocino triple junction, California: Geology, v. 11, n. 1, p. 35–39, http://dx.doi.org/10.1130/0091-7613(1983)11⟨35:TUOAMW⟩2.0.CO;2

McNeill, L. C., Goldfinger, C., Kulm, L. D., and Yeats, R. S., 2000, Tectonics of the Neogene Cascadia forearc basin: investigations of a deformed late Miocene unconformity: Geological Society of America Bulletin, v. 112, n. 8, p. 1209–1224, http://dx.doi.org/10.1130/0016-7606(2000)112⟨1209:TOTNCF⟩2.0.CO;2

Merritts, D. J., and Bull, W. B., 1989, Interpreting Quaternary uplift rates at the Mendocino triple junction, northern California, from uplifted marine terraces: Geology, v. 17, n. 11, p. 1020–1024, http://dx.doi.org/10.1130/0091-7613(1989)017⟨1020:IQURAT⟩2.3.CO;2

Montgomery, D. R., 2001, Slope distributions, threshold hillslopes, and steady-state topography: American Journal of Science, v. 301, n. 4–5, p. 432–454, http://dx.doi.org/10.2475/ajs.301.4-5.432

Montgomery, D. R., and Brandon, M. T., 2002, Topographic controls on erosion rates in tectonically active mountain ranges: Earth and Planetary Science Letters, v. 201, n. 3–4, p. 481–489, http://dx.doi.org/10.1016/S0012-821X(02)00725-2

Nishiizumi, K., Imamura, M., Caffee, M. W., Southon, J. R., Finkel, R. C., and McAnich, J., 2007, Absolute calibration of ^{10}Be AMS standards: Nuclear Instruments and Methods in Physics Research Section B: Beam Interactions with Materials and Atoms, v. 258, n. 2, p. 403–413, http://dx.doi.org/10.1016/j.nimb.2007.01.297

Ouimet, W. B., Whipple, K. X., and Granger, D. E., 2009, Beyond threshold hillslopes: Channel adjustment to base-level fall in tectonically active mountain ranges: Geology, v. 37, n. 7, p. 579–582, http://dx.doi.org/10.1130/G30013A.1

Penck, W., 1953, Morphological analysis of landforms (translated by H. Czech and K. C. Boxwell): London, MacMillan and Company, 429 p.

Personius, S. F., 1995, Late Quaternary stream incision and uplift in the forearc of the Cascadia subduction zone, western Oregon: Journal of Geophysical Research—Solid Earth, v. 100, n. B10, p. 20193–20210, http://dx.doi.org/10.1029/95JB01684

Reneau, S. L., and Dietrich, W. E., 1991, Erosion rates in the southern Oregon Coast Range: Evidence for an equilibrium between hillslope erosion and sediment yield: Earth Surface Processes and Landforms, v. 16, n. 4, p. 307–322, http://dx.doi.org/10.1002/esp.3290160405

Roering, J. J., Kirchner, J. W., and Dietrich, W. E., 2001, Hillslope evolution by nonlinear, slope-dependent transport: steady-state morphology and equilibrium adjustment timescales: Journal of Geophysical Research—Solid Earth, v. 106, n. B8, p. 16499–16513, http://dx.doi.org/10.1029/2001JB000323

Roering, J. J., Perron, J. T., and Kirchner, J. W., 2007, Functional relationships between denudation and hillslope form and relief: Earth and Planetary Science Letters, v, 264, n. 1–2, p. 245–258, http://dx.doi.org/10.1016/j.epsl.2007.09.035

Schaller, M., von Blanckenburg, F., Veldkamp, A., Tebbens, L. A., Hovius, N., and Kubik, P. W., 2002, A 30,000 yr record of erosion rates from cosmogenic ^{10}Be in Middle European river terraces: Earth and Planetary Science Letters, v. 204, n. 1–2, p. 307–320, http://dx.doi.org/10.1016/S0012-821X(02)00951-2

Schaller, M., von Blanckenburg, F., Hovius, N., Veldkamp, A., van den Berg, M. W., and Kubik, P. W., 2004, Paleoerosion rates from cosmogenic ^{10}Be in a 1.3 Ma terrace sequence: response of the river Meuse to changes in climate and rock uplift: Journal of Geology, v. 112, n. 2, p. 127–144, http://www.jstor.org/stable/10.1086/381654

Sharp, R. P., 1960, Pleistocene glaciation in the Trinity Alps of northern California: American Journal of Science, v. 258, n. 5, p. 305–340, http://dx.doi.org/10.2475/ajs.258.5.305

Stock, J., and Dietrich, W. E., 2003, Valley incision by debris flows: evidence of a topographic signature: Water Resources Research, v. 39, n. 4, 1089, http://dx.doi.org/10.1029/2001WR001057

Stone, J. O., 2000, Air pressure and cosmogenic isotope production: Journal of Geophysical Research—Solid Earth, v. 105, n. B10, p. 23753–23759, http://dx.doi.org/10.1029/2000JB900181

Stone, J. O. H., Todd, C., and Balco, G., 2004, Extraction of Al and Be from quartz for isotopic analysis: University of Washington Cosmogenic Isotope Lab, Methods and Procedures, http://depts.washington.edu/cosmolab/chem.html

von Blanckenburg, F., 2006, The control mechanisms of erosion and weathering at basin scale from cosmogenic nuclides in river sediment: Earth and Planetary Science Letters, v. 242, n. 3–4, p. 224–239, http://dx.doi.org/10.1016/j.epsl.2005.11.017

Wegmann, K. W., and Pazzaglia, F. J., 2002. Holocene strath terraces, climate change, and active tectonics: the Clearwater River basin, Olympic Peninsula, Washington State: Geological Society of America

Bulletin, v. 114, n. 6. p. 731–744, http://dx.doi.org/10.1130/0016-7606(2002)114⟨0731:HSTCCA⟩2.0.CO;2

Wilson, R. C., 1997, Normalizing rainfall/debris-flow thresholds along the U.S. Pacific Coast for long-term variations in precipitation climate *in* Chen, C. L., editor, Proceedings first international conference on debris-flow hazards mitigation: mechanics, prediction, and assessment: New York, American Society of Civil Engineers, p. 32–43.

Wobus, C., Whipple, K. X., Kirby, E., Snyder, N., Johnson, J., Spyropolou, K., Crosby, B., and Sheehan, D., 2006, Tectonics from topography: procedures, promise, and pitfalls *in* Willett, S. D., Hovius, N., Brandon, M. T., and Fisher, D. M., editors, Tectonics, Climate, and Landscape Evolution: Geological Society of America Special Papers, v. 398, p. 55–74, http://dx.doi.org/10.1130/2006.2398(04)